


# Hepatic stellate cell activation and senescence induced by intrahepatic microbiota disturbances drive progression of liver cirrhosis toward hepatocellular carcinoma

Boyuan Liu,<sup>1,2</sup> Zewei Zhou,<sup>1</sup> Yu Jin,<sup>1,2</sup> Jinying Lu,<sup>1,2</sup> Dongju Feng,<sup>1</sup> Rui Peng,<sup>3</sup> Hua Sun,<sup>4</sup> Xiaoxin Mu,<sup>5</sup> Changxian Li,<sup>5</sup> Yun Chen <sup>1,2,3</sup>

**To cite:** Liu B, Zhou Z, Jin Y, *et al.* Hepatic stellate cell activation and senescence induced by intrahepatic microbiota disturbances drive progression of liver cirrhosis toward hepatocellular carcinoma. *Journal for ImmunoTherapy of Cancer* 2022;**10**:e003069. doi:10.1136/jitc-2021-003069

► Additional supplemental material is published online only. To view, please visit the journal online (<http://dx.doi.org/10.1136/jitc-2021-003069>).

BL and ZZ are joint first authors.

Accepted 04 December 2021



© Author(s) (or their employer(s)) 2022. Re-use permitted under CC BY-NC. No commercial re-use. See rights and permissions. Published by BMJ.

For numbered affiliations see end of article.

## Correspondence to

Dr Yun Chen;  
chenyun@njmu.edu.cn

## ABSTRACT

**Background** The significance of the relationship between the microbiota and diseases is increasingly being recognized. However, the characterization of tumor microbiome and their precise molecular mechanisms through which microbiota promotes hepatocellular carcinoma (HCC) development are still unclear.

**Methods** The intrahepatic microbiota was investigated from tumor, normal adjacent tissues in 46 patients with HCC and normal hepatic tissues in 33 patients with hemangioma by 16S rRNA gene sequencing. Taxonomic composition differences in patients were evaluated using Linear discriminant analysis Effect Size (LefSe) and Phylogenetic Investigation of Communities by Reconstruction of Unobserved States (PICRUST) to predict microbial functional pathways. Associations between the most relevant taxa and clinical characteristics of HCC patients were analyzed by Spearman rank correlations. The effects of microbe on hepatic stellate cells (HSCs) activation and HCC progression were examined.

**Results** We observed intrahepatic microbiota disturbances by reduced microbial diversity in HCC. The tumor microbiota of the HCC patients with cirrhosis showed higher abundance of *Stenotrophomonas maltophilia* (*S. maltophilia*). *S. maltophilia* provoked senescence-associated secretory phenotype (SASP) in HSCs by activating TLR-4-mediated NF- $\kappa$ B signaling pathway, which in turn induced NLRP3 inflammasome complex formation and secreted various inflammatory factors in the liver, thus facilitating HCC progression in mice. Moreover, signs of SASP were also observed in the HSCs in the area of HCC with higher *S. maltophilia* enrichment arising in patients with cirrhosis.

**Conclusions** Our analysis of the hepatic microbiota revealed for the first time that patients with HCC exhibited a dysbiotic microbial community with higher *S. maltophilia* abundance, which induced the expression SASP factors of HSCs and cirrhosis in the liver, concurring in the process of hepatocarcinogenesis.

## INTRODUCTION

More than 2 million estimated new cancer cases were attributed to infectious agents

including viruses, bacteria and parasites, among which HBV or HCV infection-induced inflammation was one of the most important risk factor in hepatocellular carcinoma (HCC).<sup>1</sup> While chronic liver inflammation has been proposed to play a key role in contributing to the progression of HCC, potential pathogenic stimuli that either induce or maintain tissue inflammation and fibrosis, still remain poorly understood.<sup>2,3</sup>

Microbial host factors that are independent of tumor genome composition has been shown to have multiple effects on tumor behavior and the response to anti-cancer therapies including immunotherapy targeting PD-L1 or cytotoxic T lymphocyte-associated protein 4 (CTLA-4).<sup>4-6</sup> Accumulating evidences have suggested that the cancer-associated proinflammatory network triggered by gut microbiota dysbiosis involves liver-resident IgA-producing (IgA<sup>+</sup>) cells and NKT cells that are known to regulate HCC progression.<sup>7,8</sup> In addition to the well-studied impacts of gut microbiota, the existence of microbiota in many tumor tissues initially considered ‘sterile,’ such as lung, pancreas, prostate and breast, displayed a distinct microbiome composition in each tumor type.<sup>9,10</sup> Recent work has highlighted the importance of intratumor bacteria in influencing lung cancer development and pancreatic cancer outcomes.<sup>10-12</sup> In HCC, probiotics such as *Lactobacillus* and *Bifidobacterium* species have been found to reduce mortality in patients.<sup>13</sup> However, little is known about the human HCC microbiome composition and the roles in contributing favorably or adversely to liver cancer requires further investigation.

About 80% of cases of HCC are associated with the presence of liver cirrhosis,<sup>14</sup> the final

stage in which the contribution of the senescence associated secretory phenotype (SASP) in hepatic stellate cells (HSCs) in the development and evolution of liver disease to HCC could be relevant.<sup>15 16</sup> Cellular senescence is a stress response that develop a secretory profile composed mainly of inflammatory cytokines, chemokines matrix-remodeling factors, and growth factors, hereafter referred to as SASP. Recently, it was reported that microbial metabolite deoxycholic acid has the ability to induce the SASP in HSCs in the tumor microenvironment, suggesting that the microbiota or their derived metabolite plays a pivotal role in HCC development.<sup>17</sup>

Here, we characterized the composition of the human HCC microbiome and identified the distinct alterations in bacterial species enriched in HCC tissues, demonstrating the higher abundance of *Stenotrophomonas maltophilia* (*S. maltophilia*), one of the common multidrug-resistant opportunistic pathogens,<sup>18</sup> in the tumor microbiome of patients with liver cirrhosis in contrast to those without cirrhosis and healthy subjects. We newly investigated the effects of *S. maltophilia* on liver carcinogenesis by activating HSCs and inducing HSC SASP to secrete IL-1 $\beta$  through the TLR4/NF- $\kappa$ B/NLRP3 pathway, thereby offering new insights and an opportunity to evaluate future therapeutic strategy from the perspective of intratumor bacteria.

## MATERIALS AND METHODS

### Patient selection and specimen processing

We initially used a discovery cohort of a total of 107 samples from 46 HCC patients who underwent hepatectomy (HCC) and 33 patients of hepatic hemangioma who underwent partial hepatectomy at the First Affiliated Hospital with Nanjing Medical University (FAHNMU) between March 2019 and November 2019. A second validation cohort with 74 qualified samples including tumor tissues (n=33), normal adjacent tissues (n=27) from HCC patients and normal tissues (n=14) from hemangioma patients were analyzed from Drum Tower Hospital (DTH). Patients did not receive anticancer therapy prior to tumor sampling and those with concurrent autoimmune disease, HIV, syphilis, alcohol use/abuse or recent antibiotic treatment were excluded. Fresh or archived formalin-fixed paraffin-embedded (FFPE) specimens obtained from these patients who underwent surgical resection with curative intent were collected from FAHNMU and DTH. Data collection followed the principles outlined in the Declaration of Helsinki. Detailed clinical and pathological information on the patients are presented in online supplemental table S1.

For further details regarding the materials and methods, please refer to online supplemental information.

## RESULTS

### Bacteria are present in human HCC and normal liver tissues

The final diagnoses on the resected distinct areas of liver specimens indicated Tumor (T, n=46) and paired normal

adjacent tissue (NA, n=28) were included. Normal liver tissue (N, n=33) around the hepatic hemangioma matched for age and gender as controls were also enrolled in order to assess whether any differences of liver microbiota related to the presence of HCC could be detected (figure 1A). None of the patients had received anticancer therapy before sampling. The characteristics of the population under study are shown in online supplemental table S1.

Given the relatively low microbial biomass nature of tumors, it is critical to take multiple measures to avoid, or at least detect, any possible contamination (dust, air, human commensals, reagents, etc) in the process of profiling the intratumor microbiome. Considering contamination that might have occurred in handling and processing of the samples from the hospital, we included samples in solutions taken from the centrifuge tubes that precontaining tumor mass (without tissue). To address laboratory-borne contaminants, we also introduced negative controls including DNA extraction controls and no-template controls in PCR that were processed in parallel (figure 1B). To quantify bacterial DNA, we applied a SYBR Green-based real-time quantitative PCR assay with the universal primers 515F and 806R, which are specific for the V4 region of bacterial ribosomal 16S gene (16S rDNA (ribosomal DNA)). Levels of bacterial DNA in tissue samples were significantly higher compared with those found in the DNA extraction, PCR amplification and sample solution controls (figure 1C). To visualize and validate the presence of live bacteria in human tumors, we next used samples to isolate and culture bacteria from liver tissues (figure 1D). These colony bacteria were selected and DNA was extracted for subsequent 16S rRNA sequencing, with the results showing high abundance of bacteria within the phyla (ie, *Stenotrophomonas*, *Kroppenstedtia*, *Streptomyces*, *Staphylococcus*, *Acinetobacter*, *Brevundlmonas*, *Micrococcus*, *Bacillus*) from liver tissue samples (figure 1E). Overall, the results obtained from all of these liver samples in patients confirmed the existence of bacteria in tumor, tumor adjacent tissues and normal tissues with diverse microbiome.

### Tumor microbiome dysbiosis in HCC

To better understand the composition of tumor microbiome associated with HCC, the taxonomic profiling via 16S rRNA gene sequencing was performed on all available liver samples. Rarefaction curves were constructed for each individual sample showing the number of observed taxonomic units. After low-quality and chimeric sequences were removed, 7,294,057 (43,051–80,221) high-quality reads were obtained, which were clustered into 26,087 operational taxonomic units (OTUs) at 97% sequence similarity (online supplemental figure S1A). Relative abundance curve showed the richness and evenness of species across the samples (online supplemental figure S1B). We used different metrics to calculate microbial  $\alpha$ -diversity, including OTU species count, and the Shannon index for biodiversity. Remarkably dissimilar

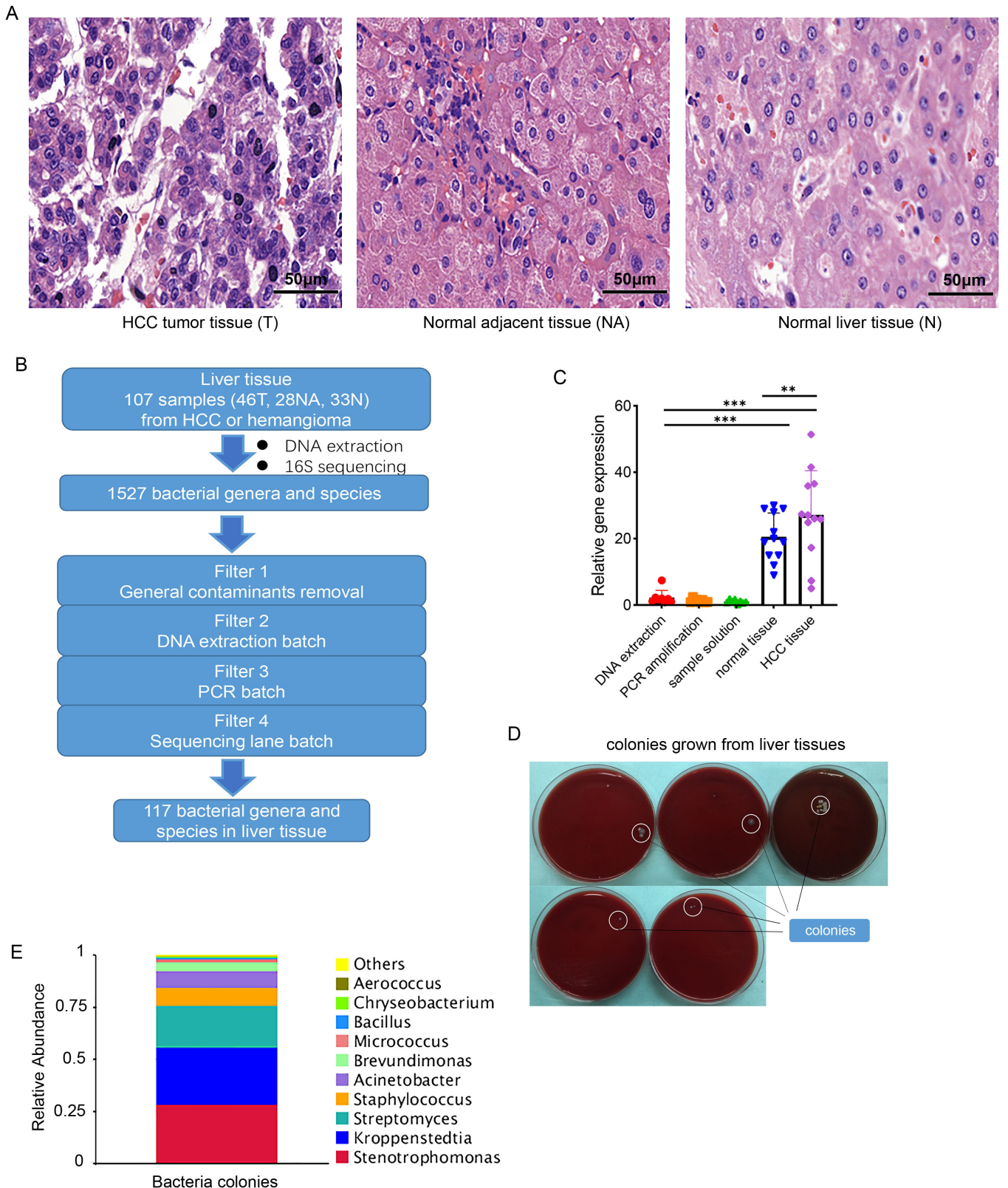


**Figure 1** Microbiota are detected and validated in liver cancer tissues. (A) Representative H&E images to identify and confirm the three different regions (Tumor, Normal adjacent and Normal regions) in HCC patients' liver. Scale bar, 50  $\mu$ m. (B) Schematic representation of the analysis pipeline applied to 16S rDNA sequencing data. (C) The presence of bacterial DNA in human tumors was assessed by bacterial 16S rDNA by qPCR. The bacterial DNA expression levels of the media exposed to the liver tissue during DNA extraction were also detected at the same time. (D) Culture-based assay from fresh liver samples. (E) 16S rRNA sequencing from colonies selected on agar plate. Data are presented as means  $\pm$  SEM. \*\* $P < 0.01$ , and \*\*\* $p < 0.001$ . One-way ANOVA test for (C). ANOVA, analysis of variance; HCC, hepatocellular carcinoma; rDNA, ribosomal DNA; qPCR, quantitative PCR.

shapes of the OTU rarefaction curves and relative abundance were observed when comparing T, NA and N groups (online supplemental figure S1C,D). All measures indicate that microbiome  $\alpha$ -diversity, defined as the number of species present within each sample, was significantly lower in patients with HCC compared with the normal liver from hemangioma patients (T vs N,  $p < 0.001$ ; T vs NA,  $p < 0.001$  and N vs NA,  $p < 0.001$  for observed species, [figure 2A](#); T vs N,  $p = 0.0035$ ; T vs NA,  $p < 0.001$  and N vs NA,  $p < 0.001$  for the Shannon index, respectively, [figure 2B](#)). Furthermore, normal adjacent tissues revealed a relatively higher diverse compared with matched tumor samples of HCC patients ( $n = 28$ ) (online supplemental figure S1E). The majority of the tumorous samples saturated around 1300–2500 species and around 800–2000 species for the paired normal adjacent samples (online supplemental figure S1F).

Moreover, a Venn diagram displays the distribution and overlaps of the differentially OTUs between groups. There are 8920 of the total 26,087 OTUs were shared among the three groups. A total of 11,216 of 16,834 OTUs were shared between the T and NA in HCC, while 4571 of 20,292 OTUs were unique for tumor tissues ([figure 2C](#)). Beta diversity was calculated using weighted UniFrac phylogenetic distance matrices, and visualized in principal coordinate analysis plots. While the tumor microbial communities exhibit phylogenetic closeness within each group of T and NA in HCC, our findings also confirm the major compositional distinction between tumor and non-tumor communities ([figure 2D](#)).

In addition, we found that levels of bacterial DNA in tumors with cirrhosis were significantly higher than those without cirrhosis in HCC patients (online supplemental figure S2A). However, the decreased trend for bacterial DNA was observed along with the progression of HCC, indicating that the tumor grade may be associated to a different microbiome microenvironment and in particular, higher-grade HCC may represent unfavorable ecological niche due to the increased necrosis and inflammation (online supplemental figure S2B). Since HBV infection or obesity are established risk factors for HCC, we next addressed whether the microbial profile was different between with and without these factors in HCC patients.  $\alpha$  and  $\beta$  diversity analysis showed no statistically significant differences in the microbiota profiles of HCC cases were observed for these potential contributors (online supplemental figure S2C,D).

Our results collectively indicate that there is a significant reduction in tumor microbial diversity in HCC. Furthermore, highly diverse microbiota suggested that alterations in the relative abundance of taxa are a major contributor for bacteria differences between tumor and non-tumor liver tissues.

#### **Stenotrophomonas were increased in the tumor microbiota of patients with HCC**

Taxonomic classification of bacterial were analyzed using the common approach of assigning sequences to

OTUs clustered by sequence similarity to existing rRNA databases.<sup>19 20</sup> We next compared enrichment of OTUs among T, NA and N groups, which revealed notable differences in microbiota relative abundance, as a per cent of reads assigned, at the various taxonomic level *Proteobacteria*, *Firmicutes*, *Bacteroidetes*, together accounting for up to 90% of sequences on average, were the dominant phyla in three groups ([figure 2E](#)). Tumorous microbial composition from three groups at the class, order, family, and species levels are presented in online supplemental figure S3A-D. The most represented genera in tumors are *Stenotrophomonas*, *Acinetobacter*, *Phyllobacterium*, and *Enterococcus* ([figure 2F](#)). In particular, HCC subjects had enrichment for specific microbes within the genus *Stenotrophomonas*, belonging to the *Proteobacteria* phylum, which are extremely rare in normal controls. *Stenotrophomonas maltophilia* was the only species of *Stenotrophomonas* genus that was consistently detected in HCC patients from T and NA tissue samples even though the relative abundances between the two groups were not significantly changed.

*S. maltophilia* is an emerging global opportunistic pathogen and associated with high fatality in immunocompromised and debilitated individuals.<sup>21</sup> Importantly, *S. maltophilia* is also a significant pathogen in patients with cancer, with the Infections including respiratory tract infections, bacteremia from bloodstream and biliary sepsis.<sup>18</sup> It has been reported that supernatants of clinical *S. maltophilia* isolates recovered from liver exhibited hemolytic and enzymatic activities, resulting in endocytosis, cell aggregation, and cytotoxicity effects on cells.<sup>22</sup> Therefore, dysbiosis may worsen with the progression of primary HCC since the presence of *S. maltophilia* by the sequencing results of our culture colonies has also been identified ([figure 1D,E](#)).

To definitively observe the presence and the location of tumorous bacteria, we performed fluorescence in situ hybridization (FISH) with specific probes to target 16S rRNA region in a subset of archival FFPE HCC cases. Additionally, in the same set of FFPE samples, we detected the immune cells by immunostaining using a CD45 antibody. The results showed that normal control liver tissues were harboring few bacteria, which were mostly within CD45<sup>+</sup> immune cells, although it is unclear if these were liver-resident bacteria or were migrated from elsewhere. However, in the tumor tissues of HCC patients, bacteria were found in the parenchyma, outside immune cells, suggesting their free translocation to the liver ([figure 2G](#)). Furthermore, considering the presence of *S. maltophilia*, one of the top species enriched in HCC versus normal controls, we used primers designed for this species and confirmed the presence of this bacterial DNA in HCC samples analyzed (online supplemental figure S3E).

Taken together, the results obtained from all of these approaches confirmed the presence of bacteria including *S. maltophilia* species enriched in the HCC samples, suspecting an expansion and migratory with enhanced invasion potential on tumor microenvironment.

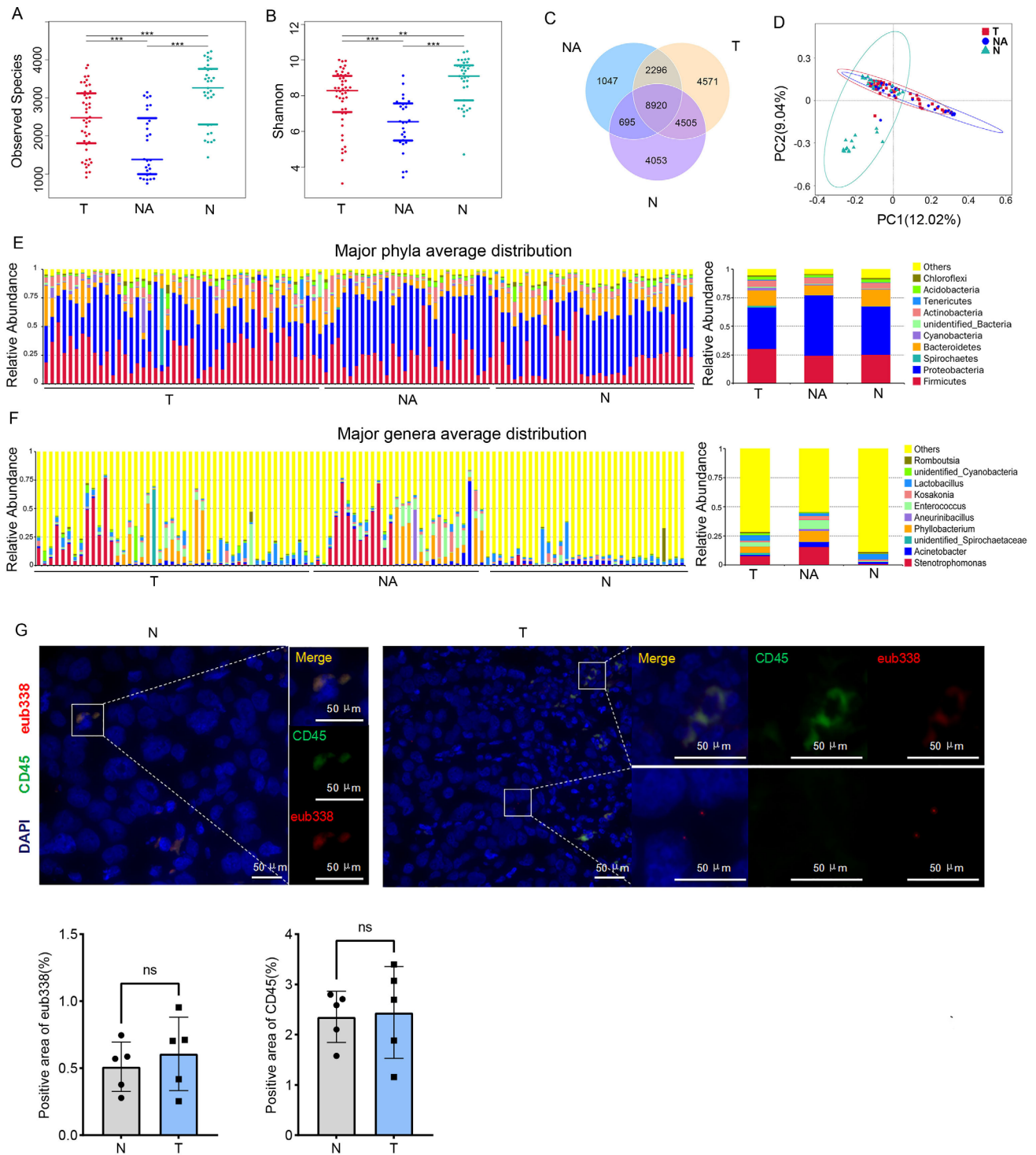


**Figure 2** Phylogenetic profiles of microbes among HCC tumor tissue (n=46), normal adjacent tissue (n=28) and normal tissue (n=33). (A, B) Compared with the N group, alpha diversity boxplot indicated as (A) Observed species and (B) Shannon index of T and NA significantly decreased. (C) A Venn diagram displaying the overlaps between three groups showed that 8920 of the total richness of 26,087 OTUs were shared among the three groups, while 13,425 of 25,040 OTUs were shared between T and N. (D) Principal coordinate analysis (PCoA) using weighted-UniFrac of beta diversity, indicating a different distribution of liver microbial community among T (red dots), NA (blue dots), and N (green dots). (E, F) Bar plots displaying taxonomic composition at the major phyla (E) and genera (F) of each sample (left) and average abundance in the T, NA and N groups (right). (G) Representative Immunofluorescence images (up) and statistical analyses (down) of normal (left) and tumor (right) liver sections stained with eub338 FISH probe (red), CD45 (green) and DAPI (blue). Side images show merged and individual staining of enlarged areas demarcated by squares in the main picture, the scale bar indicates 50  $\mu$ m. Data are presented as means  $\pm$  SEM. ns, no statistical significance, \*\* $P < 0.01$ , \*\*\* $p < 0.001$ . One-way ANOVA test for (A, B). ANOVA, analysis of variance; DAPI, 4,6-diamidino-2-phenylindole; FISH, fluorescence in situ hybridization; HCC, hepatocellular carcinoma; OTUs, operational taxonomic units.

### Identification of specific microbial taxa changes in HCC

To confirm the most relevant taxa responsible for the differences between the tumorous bacterial communities of patients with HCC and that of controls, the Linear discriminant analysis of Effect Size algorithm with a logarithmic LDA score cut-off  $> 4.0$  was then performed. We identified 10 genera for T versus N and T versus NA, which were differentially abundant in both sets of compared groups (figure 3A,B). The HCC tumors exhibited a predominance of *Firmicutes* taxa, including the genus *Enterococcus* as well as *Phyllobacterium* and the family *Enterococcaceae*. In contrast, the normal liver tissues were dominated by *Pseudomonadales* and *Rhodobacteriales* at the order level and family *Rhodobacteraceae* (figure 3A). When compared with normal adjacent tissues, microbiomes of HCC also had an enrichment in *Firmicutes* taxa, in which the genus *Lactobacillus* and family *Lactobacillaceae* were identified as being significantly enriched. Additionally, the genus *Enterococcus* and *Kosakonia*, the family *Enterococcus\_durans* and *Kosakonia\_oryzae* were the most abundant in the microbiota of tumor adjacent liver tissues (figure 3B). Since the most abundant and dominant species within a particular tissue are often crucial in regulating the microenvironment and even the response to immunotherapy,<sup>9</sup> we next compared HCC cases (T and NA group) and normal control subjects (N group) for the prevalence of specific taxa by maximum sorting method (figure 3C-E, online supplemental figure S4A-D, table S4). The abundances of 35 bacterial genera were found to be significantly different among three groups based on their median relative abundance of these taxa (top ten are shown) (figure 3C). To further investigate these findings, we focused on tumor microbial communities and conducted species comparisons that detected marked differences in the predominance of bacterial communities between T and other groups ( $p < 0.05$ ). The tumor microbiota of the HCC patients was enriched with the genus *Stenotrophomonas*, *Phyllobacterium* and *Enterococcus*, the species *Enterococcus\_durans* and *Sphingomonas\_leidy* compared with the normal controls in which *Acinetobacter* was abundant (figure 3D). When HCC tissues were compared with tumor adjacent samples, increased abundance of the genus *Lactobacillus* in tumors and *Enterococcus* in NA group were observed, but no differential species were detected (figure 3E). Although no significant difference ( $p = 0.149$ ) was observed in the abundance of *S. maltophilia* between T and NA, HCC patients was identified as having significantly higher prevalence rates of *S. maltophilia*. Taxa representing high abundance (top 10) among samples at the phylum, class, order, and family levels are shown in the online supplemental table S4A-D. We have additionally used a validation cohort, and although *Acinetobacter* and *Lactobacillus* has no significant difference, we were able to confirm the alterations of the *S. maltophilia* species which was also significantly more abundant in HCC versus normal controls (online supplemental figure S4E). Interestingly, despite the relatively low abundance, *S. maltophilia* is also present from the gut microbiome of HCC patients and healthy controls based on the previously published study (online supplemental figure S4F).<sup>23 24</sup> However, no significant difference was observed between these two groups in *S. maltophilia* from

gut microbiota, possibly indicating that nosocomial and community-acquired *S. maltophilia* infections occur in liver tissues preferentially for immunocompromised patients with HCC (online supplemental figure S4G).

Collectively, these results show that there is a significant alteration in tumor microbial diversity in HCC, with significantly higher abundance of *S. maltophilia*.

### Prediction and identification of tumor microbiome functional capacity changes in HCC

To investigate how the functional activities of intratumor bacterial community developed in HCC, we used the Phylogenetic Investigation of Communities by Reconstruction of Unobserved States (PICRUSt) approach<sup>25</sup> to map the 16S sequences to the genes and pathways that these bacterial populations may harbor. The PICRUSt analyses revealed the distinct metagenome functional content and identified 8 core predicted categories present across all liver tissue samples (figure 4A). Because the microbial communities present in patients with HCC and normal controls could be distinguished based on their functions, we next compared enrichment of differential pathways between T and NA or N groups. The functional changes in the tumor microbiomes possessed significantly increased KEGG pathways of human disease of cancer compared with N group ( $p = 0.0027$ ) (figure 4B). In addition, tumor microbiomes exhibited the decreased pathways related to metabolism of terpenoids and polyketides compared with that from normal tissues (online supplemental table S5). It has been proved that the terpenoids and polyketides have the potential anti-cancer activity against refractory ovarian, breast and other cancers.<sup>26 27</sup> In contrast, NA samples exhibited enrichment in predicted functional categories associated with diverse metabolic processes of energy, xenobiotics biodegradation and other amino acids compared with tumor microbiomes (online supplemental table S6).

The changes in predicted capability may suggest that composition of the intratumoral microbiome may influence HCC progression. Interestingly, we found a strong significant correlation between microbial function and cirrhosis that could potentially increase the occurrence and progression of HCC. Of note, TGF- $\beta$ , a key molecule in liver fibrosis, was found to be highly unregulated in HCC patients with cirrhosis from both T and NA tissues based on the microbial function prediction (figure 4C,D).

Together, taxonomic profile encoded by intratumoral bacteria represents differential enrichment of predicted functional pathways, which are associated with clinical features of cirrhosis in HCC.

### HCC-associated *Stenotrophomonas maltophilia* species as potential biomarkers for cirrhosis

We next evaluated whether the eight relevant taxa significantly enriched in HCC as indicated in figure 3D,E could be used to discriminate between normal controls and HCC. Receiver Operating Curve (ROC) analysis showed that *S. maltophilia* combined with *Phyllobacterium* and *Romboutsia* had the best performance in identifying HCC,

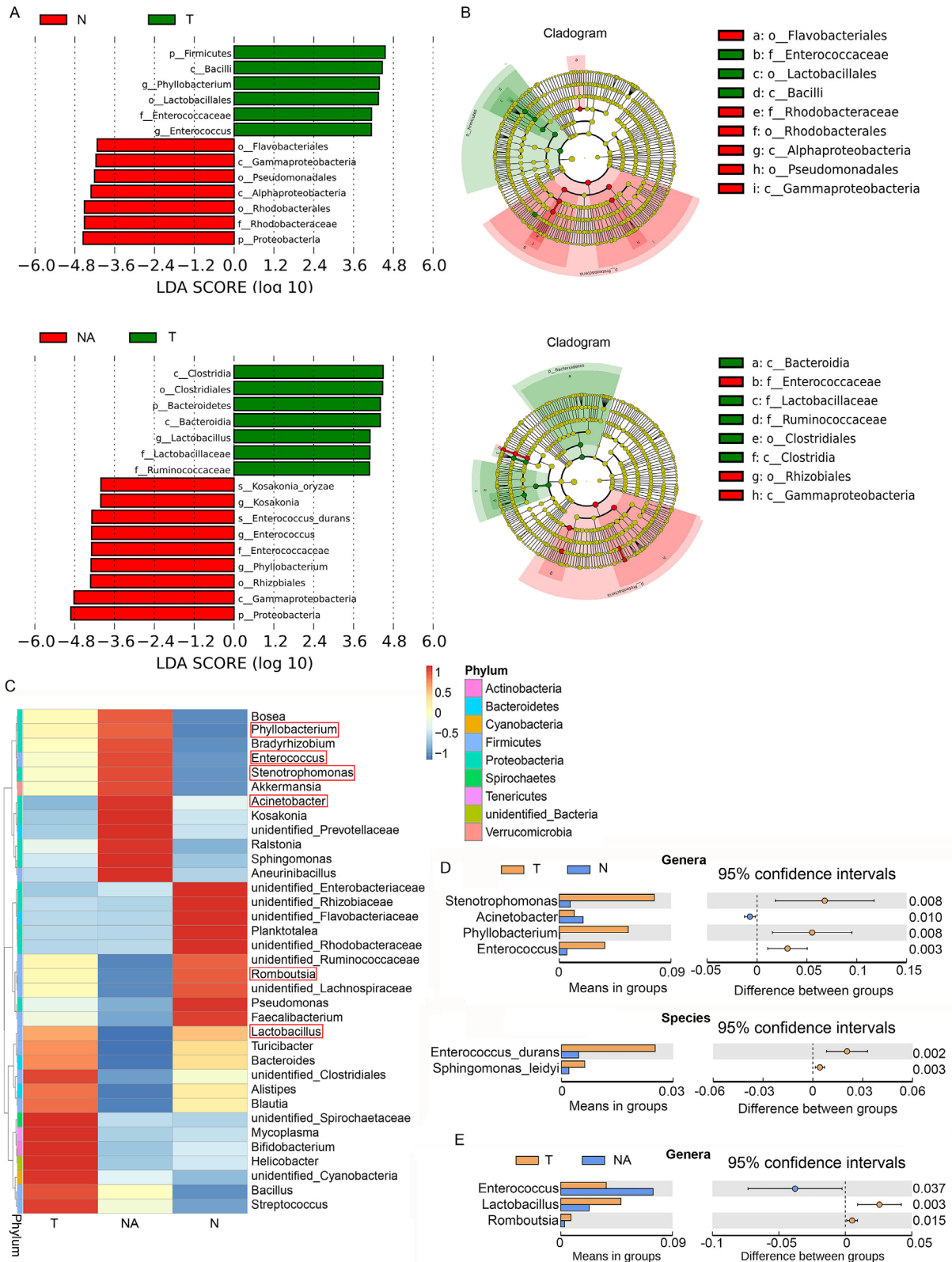


**Figure 3** Tumor microbiome communities are statistically significant differences. (A) LDA score computed from features differentially abundant between N versus T and NA versus T.\*Features with LDA score >4. (B) Taxonomic cladogram from LEfSe, depicting taxonomic association from between microbiome communities among N, NA and T groups. Each node represents a specific taxonomic type. Yellow nodes denote the taxonomic features that are not significantly differentiated between N versus T and NA versus T. Red nodes denote the taxonomic types with more abundance in N, NA groups than in T group, while the green nodes represent the taxonomic types more abundant in T group. (C) Heatmap of the selected differential bacterial abundance at the genus level in the T, NA and N groups. The red box identifies the top ten most abundant genera. (D, E) Mann-Whitney U-test of different bacteria between T versus N (D) and T versus NA (E). LEfSe, linear discriminant analysis effect size.

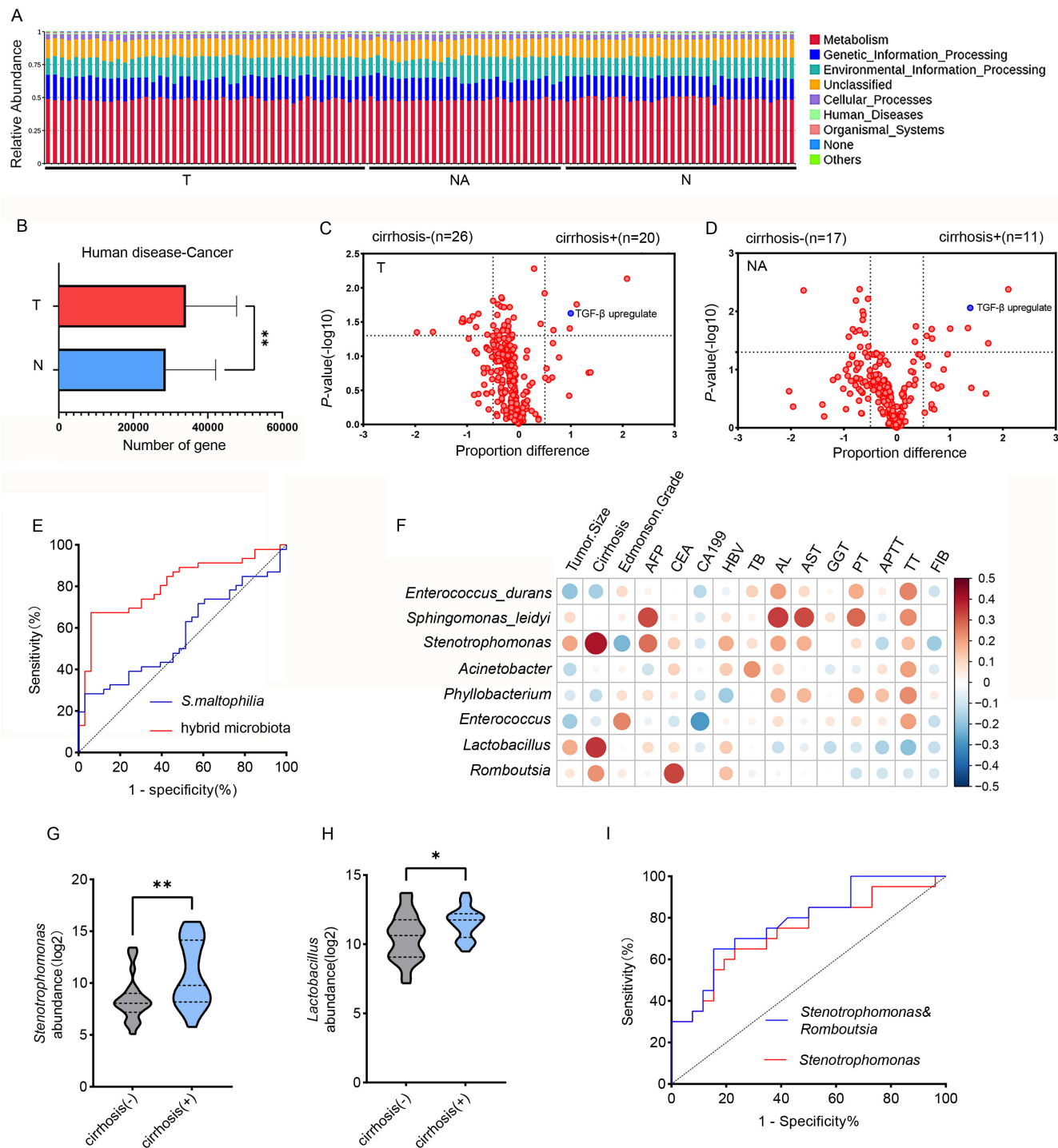


**Figure 4** Prediction and identification of tumor microbiome functional capacity changes in HCC. (A) PICRUSt analysis revealing the distinct metagenome functional content and identifying eight core predicted categories present across all liver tissue samples. (B) Functional changes in the tumor microbiomes possessed significantly increased the KEGG pathways of human disease of cancer ( $p=0.005$ ). (C, D) Volcano plots of differences in microbiota functions in HCC with or without cirrhosis samples in T (C) and NA (D). A two-sample proportion z test was used to calculate the p values. The function of TGF- $\beta$  upregulation is indicated by blue dots. (E) ROC curves analysis of *Stenotrophomonas maltophilia* combined with *Phyllobacterium* and *Romboutsia* as predictive of HCC, yielding an area under the curve (AUC) of 0.8. ( $p<0.0001$ ). (F) Person correlation analysis between eight microbiota and clinical indexes in HCC. Positive correlations are represented in red, and negative correlations are blue. The color intensity represents the strength of the correlation. (G, H) The abundance of *Stenotrophomonas* (G) or *Lactobacillus* (H) in patients with cirrhosis ( $n=20$ ) compared with those without cirrhosis ( $n=26$ ). (I) The ROC curve of *S. maltophilia* in the diagnosis of cirrhosis. Single *S. maltophilia* strains reaches an AUC value of 0.739 ( $p=0.006$ ). The maximum AUC value of 0.78 ( $p=0.001$ ) is achieved when *Romboutsia* was included. Data are presented as means $\pm$ SEM \* $p<0.05$ , \*\* $p<0.01$ . Unpaired Student's t-test was performed for (B, G, H). HCC, hepatocellular carcinoma; PICRUSt, Phylogenetic Investigation of Communities by Reconstruction of Unobserved States; ROC, receiver operating curve.



yielding an area under the curve (AUC) of 0.8 (figure 4E, online supplemental figure S5A-G).

We also performed a more detailed analysis of the eight relevant taxa in relation to clinical laboratory parameters. Several correlations were found between the enriched bacterial communities and clinical features of HCC. Notably, the enrichment of *S. maltophilia* and *Lactobacillus* in tumor tissues were positively associated with liver cirrhosis of HCC patients (figure 4F). We further stratified patients into high versus low categories based on their median relative abundance of the two taxa (*S. maltophilia* and *Lactobacillus*). We observed that patients with liver cirrhosis presented with higher abundance of *S. maltophilia* and *Lactobacillus* (figure 4G,H). Moreover, significantly liver cirrhosis was predicted for HCC patients with an enrichment of *S. maltophilia* as a biomarker using multiple logistic regression, with an AUC of 0.73 and improved to 0.78 in combination with *Romboutsia* (figure 4I).

Overall, our analysis of the tumor microbiome suggests a connection between the functions of *S. maltophilia* present in the tumor and liver cirrhosis. Considering that *S. maltophilia* were the most differentially dominant species of intratumor bacteria and these HCC patients with higher abundance had more severe disease, the pathogenicity of *S. maltophilia* possibly involved in hepatocarcinogenesis needed to be investigated.

#### ***Stenotrophomonas maltophilia* colonization of liver mediated hepatic fibrosis by inducing the HSC activation in HCC**

Activation of HSCs is now well established as the primary driver of hepatic fibrosis in human liver injury, along with the enhanced risk of HCC.<sup>28</sup> Identification of the intratumor microbiome variation by our 16S rRNA gene sequence analyses combined with our findings of a correlation between *S. maltophilia* and cirrhosis led us to test the hypothesis that *S. maltophilia* contributes to hepatic fibrosis and oncogenesis. To explore this possibility, we initially separate patients into high versus low categories based on their median relative abundance of *S. maltophilia* species. Immunohistochemistry was performed on liver biopsy samples and HCC patients with higher abundance of *S. maltophilia* showed overt HSC activation and hepatic fibrosis, as indicated by elevating the expression of  $\alpha$ -smooth muscle actin ( $\alpha$ -SMA) and Collagen I, as well as proinflammatory cytokine TGF- $\beta$  and IL-1 $\beta$  (figure 5A). Sirius red staining were also performed to assess the pathological change and showed a remarkable increase in liver fibrosis correlated with the enrichment of *S. maltophilia* (figure 5B). Furthermore, western blot analysis indicated a progressive increase in the expression of  $\alpha$ -SMA in the high category (figure 5C). Similar results were obtained from real-time PCR and showed consistently high expression of the HSC activation markers *Acta2*, *Col1a1*, *Tgfb1* and *Timp1* in patients with high abundance of *S. maltophilia* (figure 5D).

*S. maltophilia* is a Gram-negative multiple-drug-resistant organisms that can cause a wide range of infections and

invade multiple organs and tissues in humans.<sup>18</sup> Notably, *S. maltophilia* infection is of concern in patients with cancer, but little is known about their impact on cancer development.<sup>29</sup> Hence, we queried whether infection with *S. maltophilia* is capable of inducing HSC activation. HSCs LX-2 were infected with *S. maltophilia* at a multiplicity of infection of 20 for 12 hours or stimulated with the supernatant of cultured bacteria. We observed the presence of *S. maltophilia* were able to significantly induce the activation of LX-2 cells by the elevated levels of  $\alpha$ -SMA, Collagen I, TGF- $\beta$  and IL-1 $\beta$ , in contrast to untreated or mock treated with BHI medium (figure 5E). Consistently, real-time PCR results showed an elevation of pro-fibrotic factor *Acta2*, *Col1a1*, *Tgfb1* and *Timp1* in cells harboring *S. maltophilia* infection (figure 5F). In contrast, when LX-2 cells were infected with probiotic *Lactobacillus reuteri*, a negative correlation with cirrhosis, no activation was observed (figure 5E).

Thus, these results demonstrated that increased colonization with *S. maltophilia* was associated with HSC activation and fibrosis in HCC.

#### ***Stenotrophomonas maltophilia* promotes liver cancer by inducing the expression of SASP factors in senescent HSCs**

Recent studies reveal that SASP factors secreted by HSCs senescence may contribute positively cancer development.<sup>17</sup> To ascertain the role of *S. maltophilia* in SASP-associated HCC development, we first confirm that senescent cells might be present in patients with high abundance of *S. maltophilia* species. Tumor biopsy from the high categories in patients with HCC showed increased senescence-associated  $\beta$ -galactosidase (SA- $\beta$ -gal) staining (figure 6). Furthermore, a number of other senescence markers such as p16<sup>INK4a</sup> and p21<sup>CIP1</sup> expression, signs of DNA damage (53BP1 foci) and proinflammatory cytokines (IL-1 $\beta$ , Gro $\alpha$  and IL-6), were also observed in activated HSCs ( $\alpha$ -SMA-positive cells) by immunofluorescence method (figure 6B,C).

We further investigated whether Gram-positive bacteria *S. maltophilia* infection affects SASP phenotype of HSCs with subsequent fibrogenesis, and support of tumor development. As expected, primary HSCs from mice infected with *S. maltophilia* become senescent as measured by SA- $\beta$ -gal staining (figure 6D). In addition, these infected cells acquired a SASP phenotype characterized by secreting factors of Gro $\alpha$ , IL-6, IL-1 $\beta$ , p21 and HMGA1 (figure 6E). Because TLR4 are responsible for the recognition of Gram-positive bacteria and SASP is characterized by the release of inflammatory cytokines,<sup>30–32</sup> we next investigated the involvement of NLRP3 inflammasome-mediated signaling in SASP activation of HSCs and fibrosis in HCC. Indeed, treatment with *S. maltophilia* exhibited an elevated expression level of p- $\text{IKK}\alpha\beta$  (Ser180/181), caspase-1 p20 and IL-1 $\beta$  than those observed in control groups, suggesting that *S. maltophilia*-induced proinflammatory cytokine IL-1 $\beta$  via activation of TLR4/NF-Kb/NLRP3 pathway (figure 6F). However, *S. maltophilia*-induced HSC activation was attenuated by

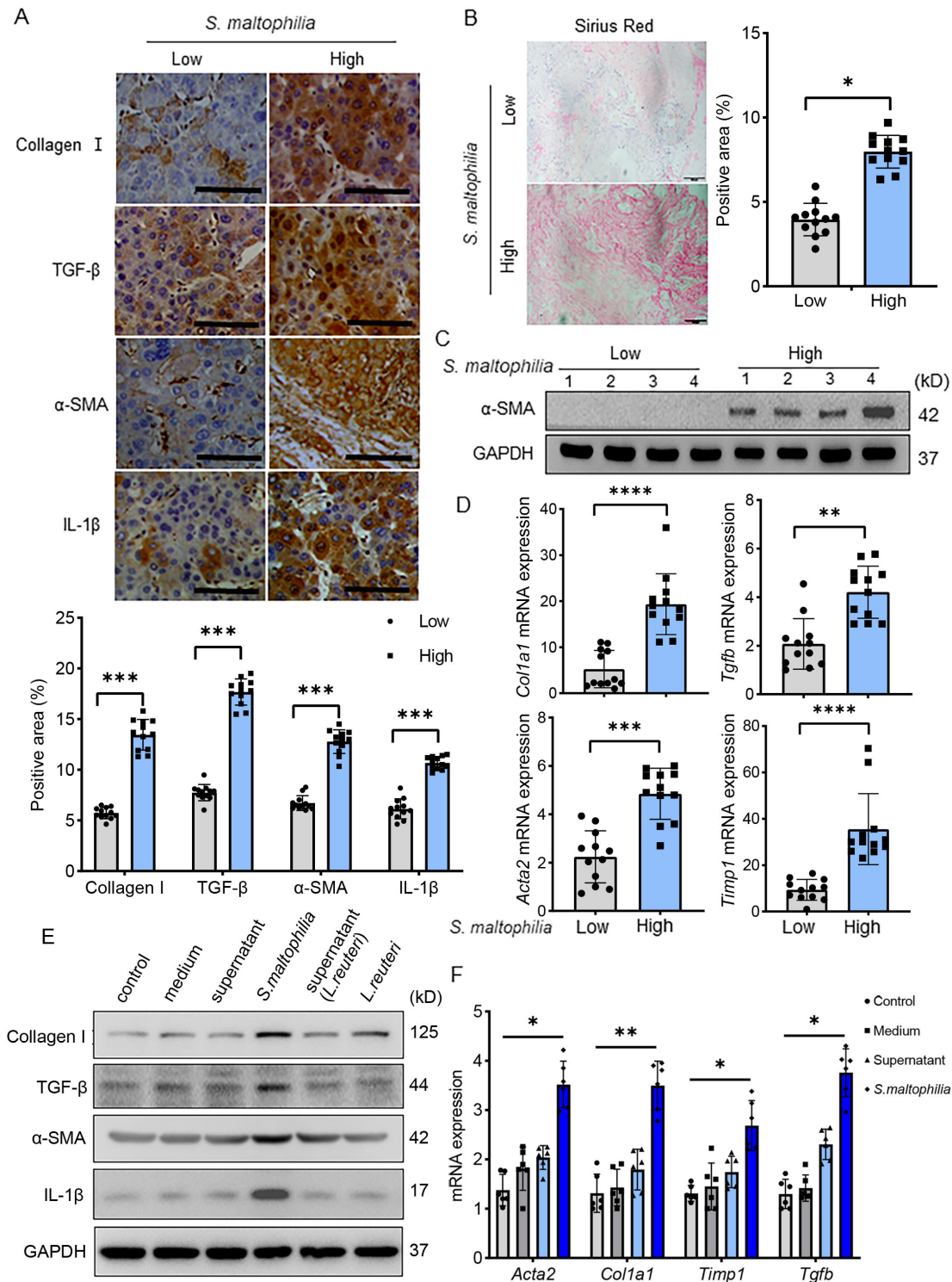


**Figure 5** *Stenotrophomonas maltophilia* mediates hepatic fibrosis by inducing the HSC activation in HCC. (A) Immunohistochemistry of Collagen I, TGF- $\beta$ ,  $\alpha$ -SMA and IL-1 $\beta$  in tumor tissue. The High group (samples with a higher abundance of *S. maltophilia*, n=12) had higher expression than that in the Low group (samples with a lower abundance of *S. maltophilia*, n=12). Scale bar, 100  $\mu$ m. (B) Fibrillar collagen deposition was evaluated in tumor tissue by Sirius red staining in the Low group (n=12) and the High group (n=12). Scale bar, 50  $\mu$ m. (C) Expression of  $\alpha$ -SMA in low and high groups were determined by Western blot analysis. Numbers in (C) indicates individual sample. (D) The levels of hepatic Col1a1, Acta2, Tgfb1 and Timp1 mRNA were measured by qPCR in the low group (n=12) and High group (n=12). (E) The expressions of Collagen I, TGF- $\beta$ ,  $\alpha$ -SMA and IL-1 $\beta$  after different stimulations were detected by Western blot in LX-2 cells. (F) The levels of Col1a1, Acta2, Tgfb1 and Timp1 mRNA were measured by qPCR after different stimulation conditions in LX-2 cells. Data are presented as means $\pm$ SEM of four independent experiments (A, B, D, F). \*P<0.05, \*\*p<0.01, \*\*\*p<0.001 and \*\*\*\*p<0.0001. Unpaired Student's t-test was performed for (A, B, D), one-way ANOVA test for (F). ANOVA, analysis of variance;  $\alpha$ -SMA,  $\alpha$ -smooth muscle actin; qPCR, quantitative PCR.

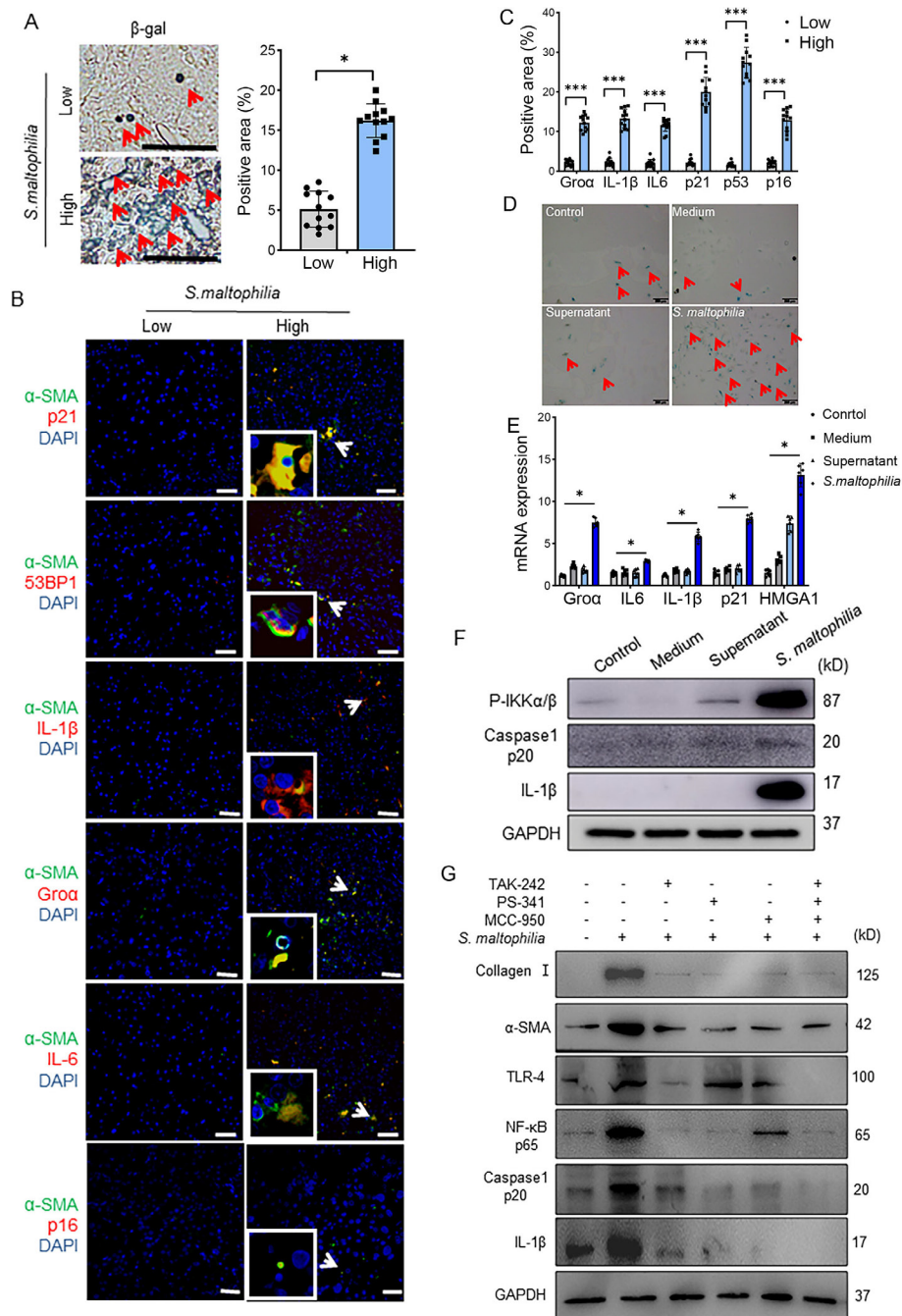


**Figure 6** *Stenotrophomonas maltophilia* induces the senescence of hepatic stellate cells and leads to inflammatory response. (A)  $\beta$ -gal staining of tumor tissue in the low (n=12) and high (n=12) group. Arrowheads indicate senescent cells that were positive for the indicated markers (cyan). Scale bar, 50  $\mu$ m. P=0.03 (B, C) Representative of immunofluorescence images (B) and quantification (C) of HSCs in liver sections between low (n=12) and high (n=12) group. HSCs were visualized by  $\alpha$ -smooth muscle actin staining ( $\alpha$ -SMA; green), and the cell nuclei were stained with 4,6-diamidino-2-phenylindole (DAPI; blue). Arrowheads indicate  $\alpha$ -SMA-expressing cells that were positive for SASPs including p21, 53BP1, IL-1 $\beta$ , Gro $\alpha$ , IL-6 and p16 (red). The histograms indicate the percentages of  $\alpha$ -SMA-expressing cells that were positive for the indicated markers. The data from three to four sections in each group are presented as the mean $\pm$ SEM. More than 100 cells in total were counted for statistical analysis. Scale bar, 50  $\mu$ m. (D) Senescent cells were identified by  $\beta$ -gal staining after various stimulations in murine primary HSCs. Arrowheads indicate senescent cells that were positive for the indicated markers (cyan). Scale bar, 200  $\mu$ m. (E) RT-qPCR analysis of the IL-6, Gro $\alpha$ , IL-1 $\beta$ , p21 and HMGA1 gene levels in murine primary HSCs after different stimulations. (F) Western blot analysis showed that the expression of P-IKK $\alpha$ / $\beta$ , IL-1 $\beta$  and caspase-1 p20 was upregulated in LX-2 cells after *S. maltophilia* stimulation. (G) Western blot analysis showed that *S. maltophilia*-induced HSC activation was attenuated by pre-treatment with the inhibitors of TLR-4 (TAK-242), NF- $\kappa$ B (Bay11-7082) and NLRP3 (MCC950) in LX-2 cells. Data are presented as means $\pm$ SEM of four independent experiments (A, C, E). \*P<0.05, \*\*\*p<0.001. Unpaired Student's t test was performed for (A, C), one-way ANOVA test for (E). ANOVA, analysis of variance; HSCs, hepatic stellate cells; RT-qPCR, hepatic stellate cells; SASPs, senescence-associated secretory phenotype.

pretreatment with the TLR-4 inhibitor TAK-242, NF- $\kappa$ B inhibitor PS-341 or/and the NLRP3 inhibitor MCC950, as evident by the decreased level of collagen I,  $\alpha$ -SMA and IL-1 $\beta$  levels (figure 6G).

### ***Stenotrophomonas maltophilia*-induced aggravation of liver fibrosis was dependent on NLRP3 signal Transduction in vivo**

We next investigated the existence of SASP activation in HSC cells induced by *S. maltophilia* infection in vivo. Mice were infected i.p. with *S. maltophilia* for 3 days and then treated with CCl<sub>4</sub> for 4 weeks to establish liver fibrosis mouse model. The local bacterial distribution of *S. maltophilia* in the liver, kidney cortex and spleen of infected mice was determined using the specific primers for *S. maltophilia* in 16S rDNA PCR and FISH analysis which demonstrated that *S. maltophilia* infected the liver in vivo with higher efficiency but hardly detected in other organs (online supplemental figure S6A,B). We next observed elevated a number of other senescence markers, such as p21<sup>CIP1</sup>, p16<sup>INK4a</sup>, 53BP1, IL-6, Gro $\alpha$  and IL-1 $\beta$  by immunohistochemistry in infected mice compared with CCl<sub>4</sub>-treatment alone, but not in the fibrosis-free control (figure 7 and online supplemental figure S6C). Similar SASP phenotype was also observed in fibrosis mice infected with *S. maltophilia* and displayed increased mRNA expression of genes encoding p21, HMGA1, IL-1 $\beta$ , Gro $\alpha$  and IL-6 and  $\alpha$ -SMA protein relative to non-infected or fibrosis-free mice (figure 7B,C). Interestingly, immunostaining with anti- $\alpha$ -SMA antibody (green) and *S. maltophilia* specific probe (red) showed a co-localization of bacteria and HSCs in liver tissues, while  $\alpha$ -SMA was undetectable in fibrosis-free mice (online supplemental figure S6D).

However, in livers from NLRP3-deficient mice, the expression of fibrosis markers, such as  $\alpha$ -SMA, Collagen I, TGF- $\beta$  and IL-1 $\beta$ , was significantly reduced even in the presence of *S. maltophilia* infection, which was also confirmed by sirius red staining demonstrating decreasing liver fibrosis (figure 7D and online supplemental figure S7A,B). Accordingly, the mRNA expression of the HSCs activation-related genes including *Acta 2*, *Col1a1* and *Timp1* was decreased or unchanged in NLRP3-deficient mice infected with or without *S. maltophili*, suggesting that NLRP3-mediated signaling induced the expression of SASP factors and fibrosis (online supplemental figure S7C). Furthermore, we also used the NLRP3, IL-1 $\beta$  and TGF- $\beta$  inhibitors separately to evaluate the effect of these SASP-related proinflammatory factors on *S. maltophilia*-inducing liver fibrosis in vivo. Consistent with the results from NLRP3-deficient mice, the mice of *S. maltophilia* infection with inhibitors treatment displayed more attenuated fibrosis and progression of HCC than those of mice infected only or without infection (figure 7 and online supplemental figure S8).

Collectively, these in vivo studies indicated that can these activated HSCs by *S. maltophilia* from liver tissues are senescencing and may promote inflammatory-associated

HCC development via SASP, which may provide a new strategy for tumor immunotherapy.

## **DISCUSSION**

Intratumor bacteria have been detected in many tumor types and displayed tumor type-specific microbiome,<sup>9 10 33</sup> but a detailed and comprehensive analysis of the microbial ecosystem of the pathologic and healthy liver tissues remains incompletely studied. In this study, we represent for the first report to characterize the microbiota composition of 107 samples (discovery cohort) and validated in another 74 samples (validation set) from human liver tissues including HCC. Because of low biomass of bacteria in tissues,<sup>9 34</sup> we performed 16S rDNA sequencing in two independent cohorts from different institutions and took measures to control for contamination to confirm the presence of a local liver-specific microbiome. Overall, we observed significant intratumor microbiome dysbiosis in patients with HCC, with significant enrichments of *S. maltophilia*. Further, the specific microbial taxa showed excellent capacity to discriminate between HCC patients with and without cirrhosis. Notably, we demonstrated for the first time that the involvement of the NF- $\kappa$ B and NLRP3 pathways leads to the SASP activation of HSCs caused by *S. maltophilia* infection, supporting a causal role for the process of fibrosis progression and hepatocarcinogenesis.

Accumulating evidence has shown that besides the significant role of gut microbiome in a wide range of human physiological functions and diseases, tumor tissues was also demonstrated the presence of a local type-specific microbiome and to be involved in tumor progression and the response to immunotherapy.<sup>22</sup> Recently, it was reported that tumor microbiome diversity and composition modulated the host immune response that ultimately influenced pancreatic cancer outcomes.<sup>10</sup> In breast cancer, a rich and diverse microbiome was detected in which colonization with *Bacteroides fragilis* strongly induced tumor growth and metastatic progression.<sup>33</sup> Our finding suggests that the HCC tumor microbiome imbalances are associated with specific clinical indicators and HSC activation that has profound influences on the HCC progression. Importantly, we observed significant differences in abundance of *S. maltophilia*, combined with *Phyllobacterium* and *Romboutsia*, can distinguish HCC patients with or without cirrhosis.

Few studies report the presence of liver microbiota,<sup>35</sup> and we have identified some bacterial taxa as selective inhabitants in HCC. In particular, increased abundance of *Streptococcus*, *Bacillus*, *Helicobacter*, and *Mycoplasma* was found in tumor tissues from patients with HCC. The gut microbiota profile of HCC patients with fibrosis have revealed higher abundance of genera *Streptococcus* and *Bacillus*.<sup>36</sup> *Streptococcus gallolyticus* from blood and ascitic fluid in patients was significantly associated with the occurrence of HCC.<sup>37</sup> Consistent with our results, previous studies have indicated the presence of *Helicobacter* species infection, known for the causative agent of

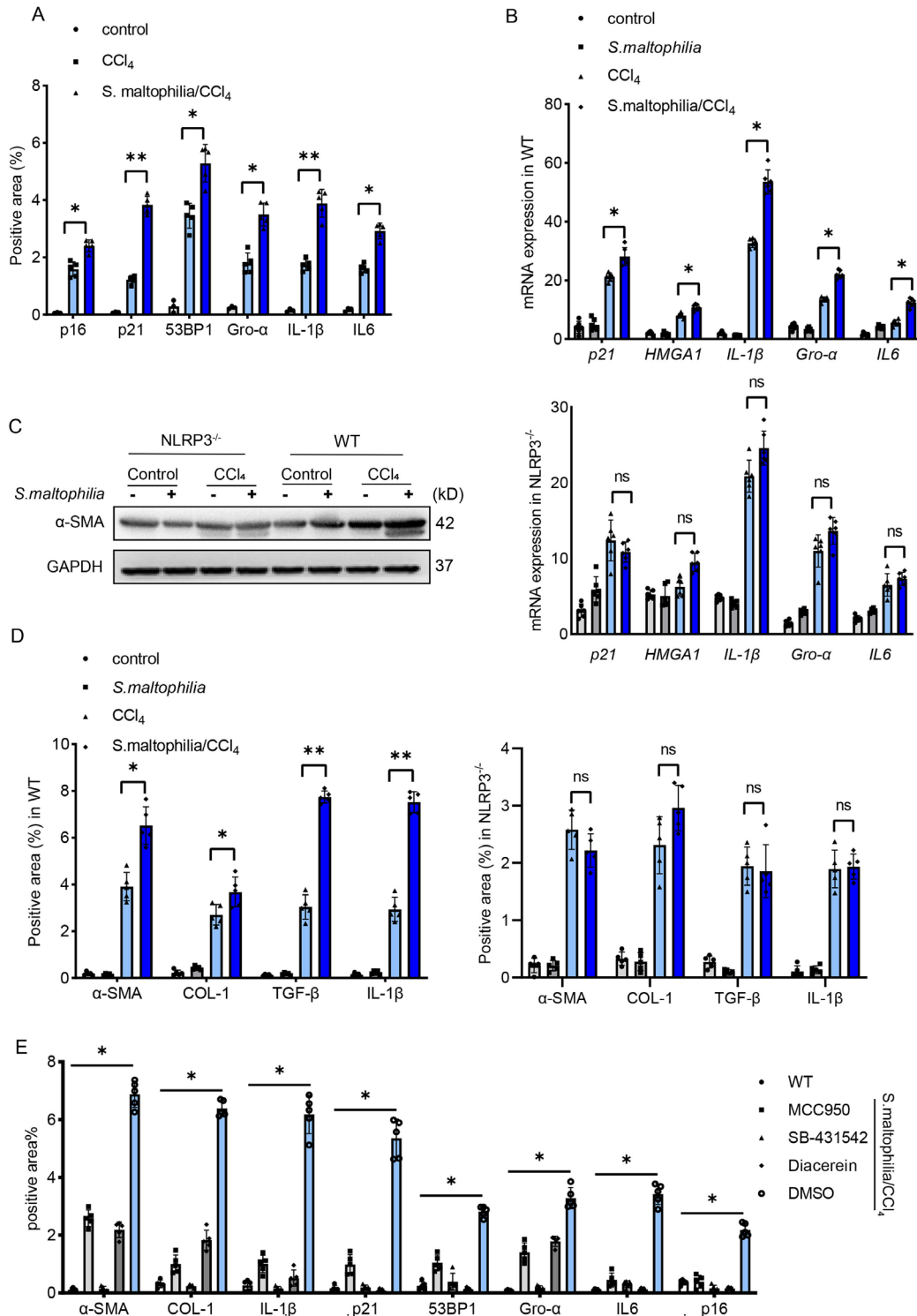


**Figure 7** *Stenotrophomonas maltophilia*-induced liver fibrosis was dependent on NLRP3 signal transduction. (A) The histograms of HSCs-positive area in mice liver, which was indicated by p21, 53BP1, IL-1 $\beta$ , Gro $\alpha$ , IL-6 and p16 detecting by Immunofluorescence. Each group had 5 mice. (B) qPCR analysis of p21, HMGA1, IL-1 $\beta$ , IL-6 and Gro $\alpha$  levels in WT or NLRP3 $^{-/-}$  mice livers after different stimulations. Each group had 5 mice. (C) The expression of  $\alpha$ -SMA was determined by Western blot in WT and NLRP3 $^{-/-}$  mice liver tissues after different stimulations. (D) Quantitative statistical charts of the expression of Collagen I, TGF- $\beta$ ,  $\alpha$ -SMA and IL-1 $\beta$  which were determined by immunohistochemistry in WT or NLRP3 $^{-/-}$  mice liver sections after different treatment. Each group had 5 mice. (E) Quantitative statistical charts of the expression of  $\alpha$ -SMA, Collagen I, IL-1 $\beta$ , p21, 53BP1, Gro $\alpha$ , IL6 and p16 in mice livers after treatment with *S. maltophilia* or together with TLR-4 inhibitor TAK-242, NF- $\kappa$ B inhibitor PS-341 or/and the NLRP3 inhibitor MCC950, which were determined by immunohistochemistry. Each group had 5 mice. \* $P < 0.05$ . Data are presented as means  $\pm$  SEM of four independent experiments (A, B, D, E). ns, no statistical significance, \* $P < 0.05$ , \*\* $p < 0.01$ . One-way ANOVA test for (A, B, D and E). ANOVA, analysis of variance;  $\alpha$ -SMA,  $\alpha$ -smooth muscle actin; HSCs, hepatic stellate cells; qPCR, hepatic stellate cells.

gastric cancer, also exists in liver tissues of HCC patients.<sup>35</sup> However, due to the limited number of cases, there is still no systematic evaluation of risk factors or clinic features associated to a different microbiome microenvironment.

HCC develops from chronically damaged liver tissue that contains sustained inflammation and fibrosis, which eventually leads to hepatocarcinogenesis. As HCC progression, their disorganized, leaky vasculature and bile duct injury may allow bacteria to enter, and the tumorous immunosuppressive microenvironment may provide a refuge for the infiltrated bacteria.<sup>38,39</sup> Moreover, gut-liver axis is widely implicated in the pathogenesis of liver diseases and most of the gut bacterial communities has the capacity to colonize multiple tumorous milieu,<sup>40,41</sup> suggesting that potentially bacterial translocation from the gut to the liver might also be occurring. We identified differences in microbial diversity and richness among the different zones of the liver, especially when comparing the tumor versus the peritumoral area, indicating bacteria colonization may modify the overall microbiome of the tumor. Additionally, FISH and immunofluorescence staining clearly demonstrated the intracellular localization of bacteria in CD45<sup>+</sup> immune cells from normal liver tissues. In contrast, the bacteria were mainly found to exist extracellularly in HCC tumors, indicating the probability of these bacteria entering established tumors via the route outside the liver. However, it must be recognized that bacteria may be colonization in the most favorable environment facilitating immune escape, irrespectively of the entry route. Future studies are necessary to clarify the origin of these specific intrahepatic bacteria and their possible pathogenic role in HCC.

Increasing evidence suggested that SASP phenotype of HSCs has crucial roles in promoting HCC development.<sup>16,17</sup> NLRP3, a key component of the inflammasome, is important for HCC progression and higher expression of NLRP3 is associated with higher grade and poor prognosis.<sup>42,43</sup> Our results advance the understanding about the molecular mechanisms underlying *S.maltophilia* and fibrosis-associated HCC progression. *S.maltophilia* provokes SASP activation in HSCs, which in turn secretes a variety of pro-inflammatory factors in the liver, thus facilitating fibrosis and HCC development. We further showed that *S.maltophilia* triggers the activation of NLRP3 via TLR4/NF- $\kappa$ B pathway in HSCs. Notably, blocking NF- $\kappa$ B signaling or NLRP3 activation efficiently prevents HSC SASP and fibrosis in HCC, indicating that intratumor bacteria *S.maltophilia*-SASP axis may contribute to pathogenic process of fibrosis-associated HCC.

In summary, we found that *S. maltophilia* accelerated cirrhosis and HCC development via HSC activation and senescence through the TLR4/NF- $\kappa$ B/ NLRP3 pathway. Our results may help identify new contributors to the pathogenesis of HCC as well as manipulation of the tumor microbiome most likely to affect tumor microenvironment and the response to immune therapy. Thus, better understanding of the organ-specific microbial taxa

offers the potential for biomarker discovery or development of novel therapies for patients.

#### Author affiliations

<sup>1</sup>Department of Immunology, Key Laboratory of Human Functional Genomics of Jiangsu Province, Nanjing Medical University, Nanjing, China

<sup>2</sup>Jiangsu Key Lab of Cancer Biomarkers, Prevention and Treatment, Collaborative Innovation Center for Cancer Personalized Medicine, Nanjing Medical University, Nanjing, China

<sup>3</sup>Department of General Surgery, Research Center for Clinical Oncology, Jiangsu Cancer Hospital, Jiangsu Institute of Cancer Research, Nanjing Medical University Affiliated Cancer Hospital, Nanjing, China

<sup>4</sup>Department of Immunology, Institute of Molecular Medicine, University of Texas Health Science Center at Houston, Houston, Texas, USA

<sup>5</sup>Liver Transplantation Center, First Affiliated Hospital of Nanjing Medical University, Nanjing, China

**Contributors** YC is responsible for the overall content as guarantor. YC conceived and designed the project. BL, ZZ and HS performed experiments and analyzed the 16s rRNA sequencing data. BL, YJ, JL and DF performed experiments, interpreted the data and prepared the figures. XM, CL and RP contributed biopsy samples and pathology analysis. YC, BL and ZZ wrote the manuscript. All authors read and approved the manuscript.

**Funding** This work was supported by project grants from The National Natural Science Foundation of China (82071767, 81772602 and 91942309 to YC; 81902445 to ZZ), Jiangsu Provincial Key Research Development Program of China (BE2018750 to YC), Key Laboratory of Emergency and Trauma, Ministry of Education (KLET-201913 to YC). The Natural Science Foundation of Jiangsu Higher Education Institutions of China (19KJB310008 to ZZ), Doctor of Mass Entrepreneurship and Innovation Program in Jiangsu Province (KY101R202040 to ZZ), Fund of Development on Science and Technology of Nanjing Medical University, China (NMUB2018006 to ZZ).

**Competing interests** None declared.

**Patient consent for publication** Not applicable.

**Ethics approval** This study was approved by the Ethics Committee of the First Affiliated Hospital with Nanjing Medical University and Drum Tower Hospital (GZR2020/09).

**Provenance and peer review** Not commissioned; externally peer reviewed.

**Data availability statement** Data are available on reasonable request.

**Supplemental material** This content has been supplied by the author(s). It has not been vetted by BMJ Publishing Group Limited (BMJ) and may not have been peer-reviewed. Any opinions or recommendations discussed are solely those of the author(s) and are not endorsed by BMJ. BMJ disclaims all liability and responsibility arising from any reliance placed on the content. Where the content includes any translated material, BMJ does not warrant the accuracy and reliability of the translations (including but not limited to local regulations, clinical guidelines, terminology, drug names and drug dosages), and is not responsible for any error and/or omissions arising from translation and adaptation or otherwise.

**Open access** This is an open access article distributed in accordance with the Creative Commons Attribution Non Commercial (CC BY-NC 4.0) license, which permits others to distribute, remix, adapt, build upon this work non-commercially, and license their derivative works on different terms, provided the original work is properly cited, appropriate credit is given, any changes made indicated, and the use is non-commercial. See <http://creativecommons.org/licenses/by-nc/4.0/>.

#### ORCID iD

Yun Chen <http://orcid.org/0000-0002-4221-6454>

#### REFERENCES

- de Martel C, Georges D, Bray F, *et al.* Global burden of cancer attributable to infections in 2018: a worldwide incidence analysis. *Lancet Glob Health* 2020;8:e180–90.
- Keenan BP, Fong L, Kelley RK. Immunotherapy in hepatocellular carcinoma: the complex interface between inflammation, fibrosis, and the immune response. *J Immunother Cancer* 2019;7:267.

- 3 Ringelhan M, Pfister D, O'Connor T, *et al.* The immunology of hepatocellular carcinoma. *Nat Immunol* 2018;19:222–32.
- 4 Kadosh E, Snir-Alkalay I, Venkatachalam A, *et al.* The gut microbiome switches mutant p53 from tumour-suppressive to oncogenic. *Nature* 2020;586:133–8.
- 5 Routy B, Le Chatelier E, Derosa L, *et al.* Gut microbiome influences efficacy of PD-1-based immunotherapy against epithelial tumors. *Science* 2018;359:91–7.
- 6 Vézizou M, Pitt JM, Daillère R, *et al.* Anticancer immunotherapy by CTLA-4 blockade relies on the gut microbiota. *Science* 2015;350:1079–84.
- 7 Shalpour S, Lin X-J, Bastian IN, *et al.* Inflammation-induced IgA+ cells dismantle anti-liver cancer immunity. *Nature* 2017;551:340–5.
- 8 Ma C, Han M, Heinrich B, *et al.* Gut microbiome-mediated bile acid metabolism regulates liver cancer via NKT cells. *Science* 2018;360 doi:10.1126/science.aan5931
- 9 Nejman D, Livyatan I, Fuks G, *et al.* The human tumor microbiome is composed of tumor type-specific intracellular bacteria. *Science* 2020;368:973–80.
- 10 Riquelme E, Zhang Y, Zhang L, *et al.* Tumor microbiome diversity and composition influence pancreatic cancer outcomes. *Cell* 2019;178:e12:795–806.
- 11 Elinav E, Garrett WS, Trinchieri G, *et al.* The cancer microbiome. *Nat Rev Cancer* 2019;19:371–6.
- 12 Jin C, Lagoudas GK, Zhao C, *et al.* Commensal microbiota promote lung cancer development via  $\gamma\delta$  T cells. *Cell* 2019;176:e16:998–1013.
- 13 Amedei A. Potential therapeutic strategies to target gut microbiota in hepatocellular carcinoma. *Hepatobiliary Surg Nutr* 2019;8:527–9.
- 14 Garrido A, Djouder N. Cirrhosis: a questioned risk factor for hepatocellular carcinoma. *Trends Cancer* 2021;7:29–36.
- 15 Lopes-Paciencia S, Saint-Germain E, Rowell M-C, *et al.* The senescence-associated secretory phenotype and its regulation. *Cytokine* 2019;117:15–22.
- 16 Yoshimoto S, Loo TM, Atarashi K, *et al.* Obesity-induced gut microbial metabolite promotes liver cancer through senescence secretome. *Nature* 2013;499:97–101.
- 17 Loo TM, Kamachi F, Watanabe Y, *et al.* Gut microbiota promotes obesity-associated liver cancer through PGE2-mediated suppression of antitumor immunity. *Cancer Discov* 2017;7:522–38.
- 18 Safdar A, Rolston KV. *Stenotrophomonas maltophilia*: changing spectrum of a serious bacterial pathogen in patients with cancer. *Clin Infect Dis* 2007;45:1602–9.
- 19 Haas BJ, Gevers D, Earl AM, *et al.* Chimeric 16S rRNA sequence formation and detection in Sanger and 454-pyrosequenced PCR amplicons. *Genome Res* 2011;21:494–504.
- 20 Wang Q, Garrity GM, Tiedje JM, *et al.* Naive Bayesian classifier for rapid assignment of rRNA sequences into the new bacterial taxonomy. *Appl Environ Microbiol* 2007;73:5261–7.
- 21 An S-Q, Berg G. *Stenotrophomonas maltophilia*. *Trends Microbiol* 2018;26:637–8.
- 22 Figueirêdo PMS, Furumura MT, Santos AM, *et al.* Cytotoxic activity of clinical *Stenotrophomonas maltophilia*. *Lett Appl Microbiol* 2006;43:443–9.
- 23 Ren Z, Li A, Jiang J, *et al.* Gut microbiome analysis as a tool towards targeted non-invasive biomarkers for early hepatocellular carcinoma. *Gut* 2019;68:1014–23.
- 24 Liu Q, Li F, Zhuang Y, *et al.* Alteration in gut microbiota associated with hepatitis B and non-hepatitis virus related hepatocellular carcinoma. *Gut Pathog* 2019;11:1.
- 25 Langille MGI, Zaneveld J, Caporaso JG, *et al.* Predictive functional profiling of microbial communities using 16S rRNA marker gene sequences. *Nat Biotechnol* 2013;31:814–21.
- 26 Ateba SB, Mvondo MA, Ngeu ST, *et al.* Natural terpenoids against female breast cancer: a 5-year recent research. *Curr Med Chem* 2018;25:3162–213.
- 27 Isobe Y, Okumura M, McGregor LM, *et al.* Manumycin polyketides act as molecular glues between UBR7 and p53. *Nat Chem Biol* 2020;16:1189–98.
- 28 Myojin Y, Hikita H, Sugiyama M, *et al.* Hepatic stellate cells in hepatocellular carcinoma promote tumor growth via growth differentiation factor 15 production. *Gastroenterology* 2021;160:1741–54.
- 29 Ansari SR, Hanna H, Hachem R, *et al.* Risk factors for infections with multidrug-resistant *Stenotrophomonas maltophilia* in patients with cancer. *Cancer* 2007;109:2615–22.
- 30 Liu D, Richardson G, Benli FM, *et al.* Inflammation in the cardiovascular system: mechanisms, emerging targets, and novel therapeutic strategies. *Clin Sci* 2020;134:2243–62.
- 31 Benbow JH, Thompson KJ, Cope HL, *et al.* Diet-induced obesity enhances progression of hepatocellular carcinoma through tenascin-C/toll-like receptor 4 signaling. *Am J Pathol* 2016;186:145–58.
- 32 Wu L, Li J, Feng J, *et al.* Crosstalk between PPARs and gut microbiota in NAFLD. *Biomed Pharmacother* 2021;136:111255.
- 33 Parida S, Wu S, Siddharth S, *et al.* A procarcinogenic colon microbe promotes breast tumorigenesis and metastatic progression and concomitantly activates Notch and  $\beta$ -catenin axes. *Cancer Discov* 2021;11:1138–57.
- 34 de Goffau MC, Lager S, Sovio U, *et al.* Human placenta has no microbiome but can contain potential pathogens. *Nature* 2019;572:329–34.
- 35 Xuan S-Y, Li N, Qiang X, *et al.* Helicobacter infection in hepatocellular carcinoma tissue. *World J Gastroenterol* 2006;12:2335–40.
- 36 Ponziani FR, Bhouri S, Castelli C, *et al.* Hepatocellular carcinoma is associated with gut microbiota profile and inflammation in nonalcoholic fatty liver disease. *Hepatology* 2019;69:107–20.
- 37 Kale P, Khillan V, Sarin SK. Novel association of *Streptococcus gallolyticus* subspecies *pasteurianus* and hepatocellular carcinoma: opening new frontiers. *Scand J Gastroenterol* 2018;53:1354–7.
- 38 Font-Burgada J, Shalpour S, Ramaswamy S, *et al.* Hybrid periportal hepatocytes regenerate the injured liver without giving rise to cancer. *Cell* 2015;162:766–79.
- 39 Zhang W, Liu Y, Yan Z, *et al.* IL-6 promotes PD-L1 expression in monocytes and macrophages by decreasing protein tyrosine phosphatase receptor type O expression in human hepatocellular carcinoma. *J Immunother Cancer* 2020;8:e000285.
- 40 Human Microbiome Project Consortium. A framework for human microbiome research. *Nature* 2012;486:215–21.
- 41 Lloyd-Price J, Mahurkar A, Rahnavard G, *et al.* Strains, functions and dynamics in the expanded human microbiome project. *Nature* 2017;550:61–6.
- 42 Zhang Q, Wang H, Mao C, *et al.* Fatty acid oxidation contributes to IL-1 $\beta$  secretion in M2 macrophages and promotes macrophage-mediated tumor cell migration. *Mol Immunol* 2018;94:27–35.
- 43 Wang X, Jia Y, Wen L, *et al.* *Porphyromonas gingivalis* promotes colorectal carcinoma by activating the hematopoietic NLRP3 inflammasome. *Cancer Res* 2021;81:2745–59.